Defect dynamics in a smectic Grandjean-Cano wedge

Christophe Blanc,[1,2,*] Nadia Zuodar,[3] Ioannis Lelidis,[4] Maurice Kleman,[2,†] and Jean-Luc Martin[3,‡]
[1]*GDPC (UMR 5581) CNRS, Université de Montpellier-II, CC026, Place Eugène Bataillon, F-34095 Montpellier Cedex 05, France*
[2]*LMCP (UMR 7590), Université Pierre-et-Marie Curie, T16 Case 115, 4 Place Jussieu, F-75252 Paris Cedex 05, France*
[3]*IPMC, Swiss Federal Institute of Technology, CH-1015 Lausanne, Switzerland*
[4]*LPMC Université de Picardie, 80039 Amiens, France*
(Received 2 September 2003; published 30 January 2004)

An array of edge dislocation forms spontaneously in a Grandjean-Cano wedge filled by a smectic liquid crystal. In the vicinity of the smectic *A* to smectic *C* transition, these defects are visible under the microscope [R. B. Meyer, B. Stebler, and S. T. Lagerwall, Phys. Rev. Lett. **41**, 1393 (1978)]. This paper deals with their dynamics under controlled deformation (dilation and compression). First, we characterize several regimes of dislocation mobility occurring with increasing strain ϵ or strain rate $\dot{\epsilon}$. We relate these regimes to the interactions between screw and edge dislocations. We also show that screw dislocations give rise to loops of edge dislocations under sufficient strain, which strengthens the model of loop nucleation by helical instability of screw dislocations. Lastly, we discuss several models for the microscopic origin of the interactions between defects.

DOI: 10.1103/PhysRevE.69.011705 PACS number(s): 61.30.Jf, 46.35.+z, 61.72.Ff, 61.72.Lk

I. INTRODUCTION

It is well established that the plasticity of solids is controlled by the motion through the crystal of topological defects under stress. In the early days of crystal plasticity, Orowan [1] expressed the deformation ϵ of a crystal in terms of dislocation displacements:

$$\epsilon = A\rho_m bL, \tag{1}$$

where A is a geometric coefficient. The corresponding crystal is assumed to deform via a density ρ_m of mobile dislocations, with b and L as average dislocation Burgers vector and mean free path, respectively. Taking the time derivative of Eq. (1) under steady-state conditions (ρ_m constant with time), the deformation rate is

$$\dot{\epsilon} = A\rho_m bv, \tag{2}$$

v being the average dislocation velocity. Relation (2) is commonly called the Orowan equation.

Today, an impressive body of data is available, from plasticity studies of a variety of crystals, under a range of experimental conditions, in which the strain rate is either imposed or measured. However, the relative contributions of v and ρ_m to the deformation rate in Eq. (2) are still an open question. In other words, for a given strain rate, it is not possible to predict which combination of ρ_m and v is operating among an infinite number of possibilities [2].

As a matter of fact, when the first structural observations in crystals became possible using the transmission electron microscope (TEM), static as well as dynamic observations of dislocations were reported [3]. Dynamic experiments then developed and a body of new data was collected about moving defect lines under given deformation conditions. These included information on the aspects of dislocation motion (''jerky'' as opposed to ''viscous''), their velocities, the identification of obstacles to their motion, and details about the corresponding by-passing mechanisms. This significantly improved the understanding of crystal plasticity (see, e.g., [4]). However, although the above experiments benefited from the high spatial resolution of TEM, the restricted field of observation did not facilitate averaging the deformation parameter values over the crystal. The approach of the physical metallurgist was attempted with liquid crystals with the idea of collecting macroscopic data about the rheology of a smectic material and observing at the same time the details of defect dynamics, using an optical microscope.

Smectic liquid crystals [5] are crystals of parallel layers of two-dimensional liquids, which also display topological defects like screw and edge dislocations [6,7]. It is now established through several studies of microplasticity [8] that dislocations also control the deformation of a smectic sample (at least for small strains). But due to lack of *in situ* observations little is known about their behavior under stress, their nucleation or their interactions, unlike solid crystals. For example, recent experiments [9,10] on the dynamics of oscillatory plastic flow [11,12] in smectic liquid crystals observed in layer-normal stress experiments have been interpreted as the helical instability of screw dislocations giving rise to edge dislocations [13,14], but up to now no such instabilities have been directly shown. Edge dislocations in the smectics have, however, been directly observed under the microscope in various experimental situations: in lyotropic lamellar phases [15] or in ferrosmectics [16] between a spherical lens and a plane, in the neighborhood of the smectic A(SmA) to smectic C(SmC) transition [17] in a Grandjean-Cano wedge geometry. In the latter case, sketched in Fig. 1, the contrast of the dislocation is enhanced by the fact that the molecules are normal to the layers in the SmA phase, whereas they are tilted in the SmC phase. The local compression of the layers

*Electronic address: blanc@gdpc.univ-montp2.fr
†Electronic address: kleman@lmcp.jussieu.fr
‡Electronic address: jean-luc.martin@epfl.ch

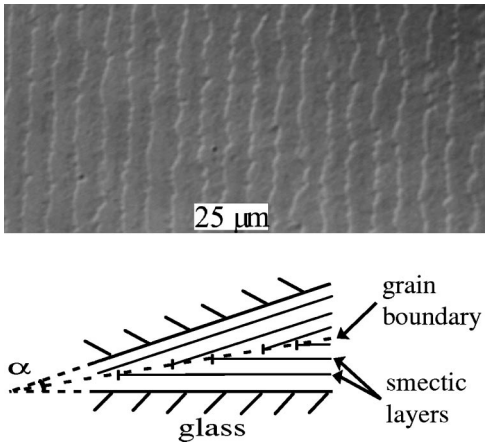

FIG. 1. A grain boundary made of a network of parallel edge dislocations is present in a Sm*A* liquid crystal confined in a Grandjean-Cano wedge. In the vicinity of the Sm*A*-Sm*C* transition, the shift of the transition temperature due to the local stress makes the edge dislocations visible under the optical microscope.

in the vicinity of a dislocation yields a local shift of the Sm*A*-Sm*C* transition. Under a polarizing microscope the Sm*C* domains (and thus the dislocations) appear clearly within the dark background of the homeotropic Sm*A* domains.

Note that all the reported observations of dislocations have concerned only motionless dislocations in samples at rest, except for some observations in free-standing smectic-*A* films [18,19].

Gathering these different ideas and observations has led us to perform microplasticity experiments of smectics, in which we can observe moving edge dislocations over large distances in order to visualize their local shapes and their interactions with other defects, and to check the Orowan equation directly.

The outline of this paper is as follows. In Sec. II, we describe the experimental setup. In Sec. III, we successively give experimental results and discuss the existence of a yield stress in smectics, study the conditions in which the Orowan equation is satisfied and the transition from a jerky to a viscous regime, and report dislocation multiplication. In Sec. IV, in the light of our results, we discuss some aspects of the interactions between edge and screw dislocations in bulk smectic liquid crystals.

II. EXPERIMENTS

A. Experimental system

The thermotropic liquid crystal we have used is a fluorinated octyloxyphenyl octyloxybenzoate (BDH173; see the structure in Fig. 2), which exhibits a Sm*A*-Sm*C* transition (when cooled from the Sm*A* phase) at 54 °C and a Sm*A*-isotropic transition at 79 °C.

The deformation microdevice (see Fig. 3) is a rigid metallic frame on which a piezoelectric ceramic (Quartz & Silica) is glued by means of a cyanocrylate contact glue [20,21]. The ceramic controls the thickness of a Grandjean-Cano wedge (of angle α) made of two flat glass plates between which the liquid crystal is confined. A high-voltage signal (obtained by a function generator and a voltage amplifier) is applied to the ceramic. We mainly use an alternating linear sweep with constant amplitude (600 V) and variable frequency ν which yields a displacement within the range 0–200 nm; the best strain obtained is of order $\times 10^{-2}$ for a 10 μm thick sample.

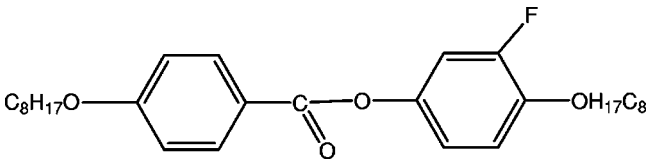

FIG. 2. Fluorinated liquid crystal used in the experiments.

The whole cell is enclosed in a millikelvin Instec oven (temperature regulated at $\pm 2\times 10^{-3}$ K) and observed under an optical polarizing microscope (Leica DMRP). The video acquisition line comprises a three-charge-coupled device 3CCD camera, a video recorder, and a PC frame grabber.

B. Sample preparation

In order to provide a good homeotropic alignment of the layers on the glass, the plates are initially coated by a monolayer of ionic surfactant cetylpyridinium chloride (CPCl; Aldrich) obtained by spin-coating of a 0.1 wt % weight solution of CPCl in ethanol [22]. Depending on the perfection of the glass cleaning, the density of screw dislocations which appear in the sample (see below) can be roughly adjusted.

The geometrical parameters of the wedge (thickness close to 10 μm and angle α) are adjusted at 54 °C under the microscope by means of precision screws. The angle α is controlled by interferometry (air wedge fringes) and fixed between 2×10^{-5} and 10^{-3} rad. The Grandjean-Cano wedge is then heated to 100 °C and filled under the microscope by the capillar flow of the liquid crystal in its isotropic phase. The sample is then slowly cooled down to the Sm*A* phase, where the homeotropic alignment is checked. We then stabilize the temperature a few tenths of degrees above the Sm*A*-Sm*C* transition when the dislocations are visible within the Sm*A* phase.

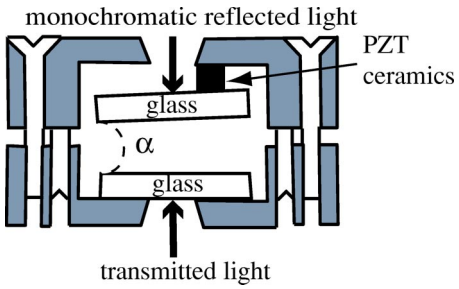

FIG. 3. Deformation microdevice: the distance between the glass plates is modified by tuning the voltage applied to the ceramic. The actual displacement is measured by interferometry of the air wedge under monochromatic reflected light (Hg green light). Vertical arrows indicate the direction of the transmitted light and of the monochromatic light used in reflection. PZT indicates the piezoelectric transducer.

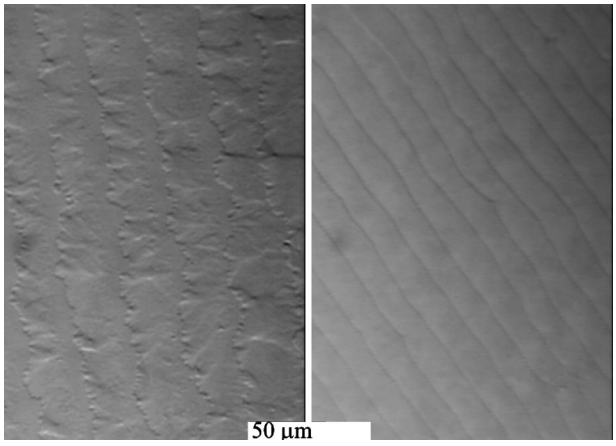

FIG. 4. Depending on the preparation of the glass, edge dislocations appear strongly pinned on numerous dots (on the left) or as straight lines (on the right). The thickness of the sample is close to 10 μm in both cases, and the edge dislocations are in the same focus plane, located at equal distances from the two glass plates. Note that slight strain might be present in the samples at rest because of the presence of a yield stress (see below).

Due to the thermal dilation of the cell and the filling of the liquid crystal, the angle α is usually slightly different in the empty and in the filled cell at the working temperature. We therefore only partially fill the wedge and leave an air wedge, which is used to measure α and the thickness variation of the stressed sample by interferometry. Note that this latter measurement is necessary to calibrate the deformation-voltage relation because the holder has a finite rigidity, and the deformation of the ceramic (≈ 0.4 nm V^{-1}) is not entirely transmitted to the sample [23].

III. RESULTS

Similarly to what has been observed in former studies [17], the edge dislocations at rest form a stable network of parallel lines. They are not usually straight, but are strongly pinned on dots of size smaller than the optical resolution. These dots are present in the sample with a typical density $N_s \approx 10^{11}$ m^{-2} [24]. Depending very sensitively on the glass cleaning, this density can be lowered to $N_s \approx 10^9$ m^{-2} (as shown in Fig. 4). Because these dots are not dragged by the moving dislocations, we think that they reveal the presence of screw dislocations that are strongly anchored on both boundary surfaces and interact with the edge dislocations (this point will be further discussed in Sec. IV; see also [25]).

The measurement of both the period p of the network and the angle α provides the Burgers vector of the dislocations,

$$b \approx p\alpha \approx 3.7 \pm 0.4 \text{ nm} \tag{3}$$

(the large relative error is due to the variation, $\approx 10\%$ for $\alpha \approx 10^{-4}$ rad, of the angle of the wedge through the sample). This value compares well with the SmA layer thickness δ measured by small angle x-ray scattering. $\delta \approx 3.3$ nm. Therefore, the edge dislocations present in the sample are elementary ones.

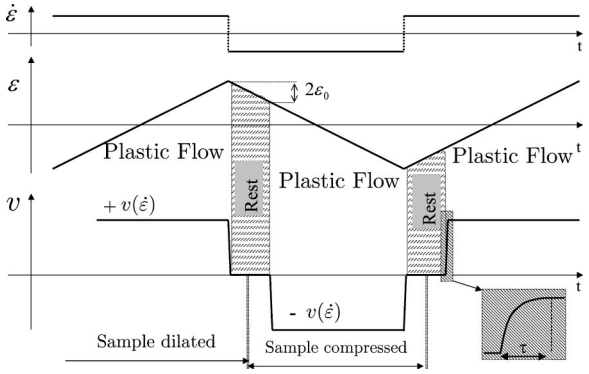

FIG. 5. Sketch of the sequence of regimes observed when a periodic triangular signal is applied. ε_0 is the value of the yield strain, $v(\dot{\varepsilon})$ is the stationary velocity of the edge dislocations at the strain rate $\dot{\varepsilon}$, and τ is the relaxation time due to the finite mobility of dislocations (see below in the text).

When a signal is applied to the piezo actuators, different types of dislocation motions are observed, depending on the strain ϵ and the strain rate $\dot{\epsilon}$. We usually work at constant strain rate by applying ramps (periodic triangular signals). At low strain (and consequently at low normal stress), no motion is observed and the dislocations are strongly pinned on dots. At higher strains, they move and relax the external stress but the motion strongly depends on the strain rate and the value of the angle α (see Fig. 5). We now detail these different regimes.

Note that in the following text we will use classical concepts from linear elasticity used in metallurgy. The normal local stress on the layers, σ, is thus given by Hooke's law: $\sigma = B\epsilon_l$ where ϵ_l is the local strain of the layers and B the compression modulus. This approach for smectic materials is relevant only when their deformation remains small, which is the case in our experiments.

A. Small strains and pinning dots

1. Observation of a yield strain

Below a finite strain ϵ_0 (for a given cell), the dislocations do not move under the applied stress but appear strongly pinned on the dots. The only effect of a compression (or a dilation) of the sample is an increase (or decrease) of the optical contrast (see Fig. 6). This effect is due to a shift of the SmA-SmC transition temperature under strain (see the detailed explanation in Ref. [17]), which increases (decreases) the width of the line.

The yield strain could not be accurately measured from the single deformation of a sample at rest, because a preexisting stress can always be present. We therefore obtained the yield strain ϵ_0 from the periods of rest of the dislocations submitted to the periodic triangular signal (see Fig. 5), which successively increases and decreases the thickness of the sample at constant strain rate ($\dot{\epsilon}$ and $-\dot{\epsilon}$). For each given cell, we found that the yield strain ϵ_0 is independent of the applied strain rate $\dot{\epsilon}$. It varies strongly, however, in the different cells (as shown in Table I) and increases with the density N_s of observable pinning points.

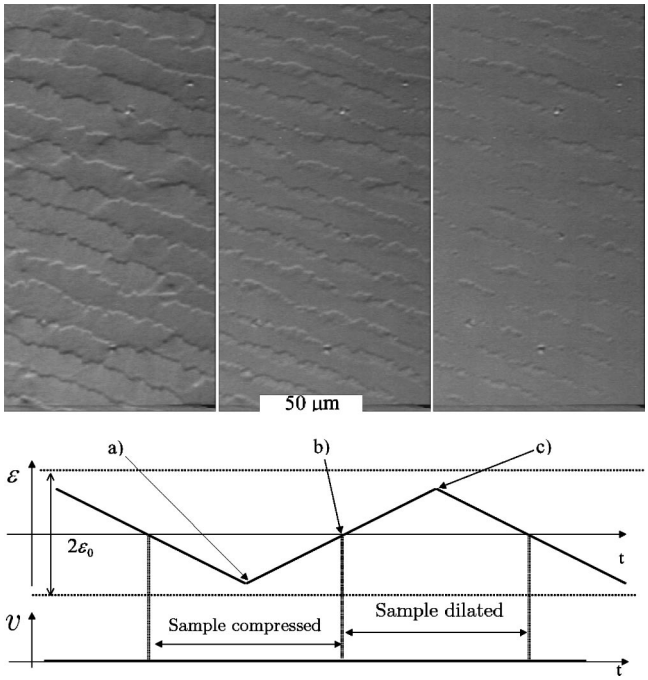

FIG. 6. Below the yield strain ϵ_0, dislocations are motionless (b). A compression (a) or a dilation (c) increases or decreases the optical contrast only, by locally shifting the Sm*A*-Sm*C* transition [17].

2. Interpretation: Origin of the yield strain

Our observations strongly suggest that the yield strain of a smectic sample is due to the presence of the pinning dots which oppose the stress induced climb of edge dislocations.

In order to relate the yield strain to the pinning dots, we first consider the case of an edge dislocation pinned only at the origin, as shown in Fig. 7. Far from the pinning dot, the dislocation rests at the distance Y_0, its equilibrium position. At the point (x,y), we denote by θ the local angle between the dislocation and the $\hat{\mathbf{x}}$ axis (see the notation in Fig. 7).

Due to the presence of the Grandjean-Cano wedge angle α, the local normal stress is given by $\sigma = B\alpha(Y_0 - y)/e$, where e is the thickness of the sample. An elementary Peach and Koehler (PK) [26] force acts on an elementary length ds of the edge dislocation when the latter departs from Y_0:

$$d\mathbf{F}_{PK} = \frac{Bb\alpha(Y_0 - y)}{e} ds\hat{\mathbf{n}}, \tag{4}$$

TABLE I. Variation of the yield strain ϵ_0 with the density N_s of pinning points in four different cells.

Sample	$p(\mu\text{m})$	$N_s(\mu\text{m}^{-2})$	ϵ_0
I [a]	22.5	8×10^{-2}	3×10^{-3}
II	23.2	2×10^{-2}	7×10^{-4}
III [b]	12.7	8×10^{-4}	1×10^{-4}
IV [c]	6.7	$\approx10^{-2}$–5×10^{-2}	5×10^{-4}

[a]See Fig. 4 left.

[b]See Fig. 4 right.

[c]The small value of p made the measurement of N_s imprecise.

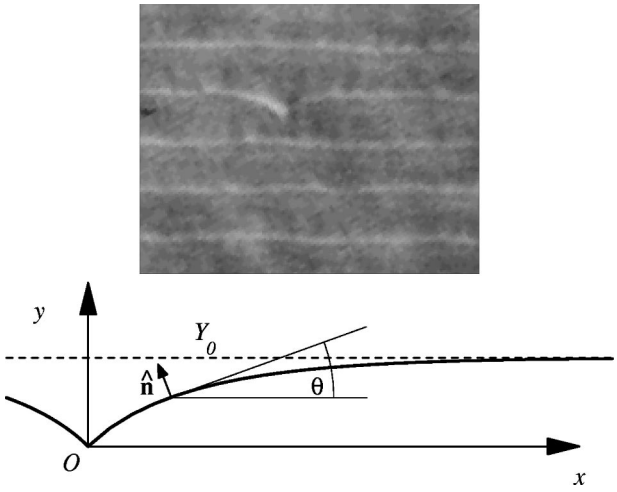

FIG. 7. Top: Isolated pinning point in sample III (period 12.7 μm). Bottom: Corresponding notation used in the text.

where $\hat{\mathbf{n}}$ is a unit vector normal to the dislocation, and $b = \delta$, the modulus of the Burgers vector along $\mathbf{n}$. The PK force is opposed to the force due to the curvature of the dislocation,

$$d\mathbf{F}_c = -\gamma \frac{d\theta}{ds} ds\hat{\mathbf{n}}, \tag{5}$$

where γ is the line tension of the dislocation. The integration of the equilibrium condition $d\mathbf{F}_c = -d\mathbf{F}_{PK}$ gives the shape of the dislocation:

$$1 - \cos\theta = \frac{Bb\alpha}{2e\gamma}(Y_0 - y)^2. \tag{6}$$

The resulting force acting on the pinning dot is given by $\mathbf{F}_\gamma = 2\gamma \sin\theta_0 \hat{\mathbf{y}}$. The depinning therefore occurs when $\theta_0 = \theta_{0,m} = \arcsin(\mathcal{F}/2\gamma)$, where $\mathcal{F}$ is the maximum force supported by the pinning dot (if $\mathcal{F} > 2\gamma$ the edge dislocation surrounds the dot for $\theta_0 = \pi/2$). The depinning therefore occurs when the dislocation is at a distance $Y_{0,m} = \mathcal{L}\sqrt{1-\cos\theta_{0,m}}$ from the dot, where $\mathcal{L} = \sqrt{2\gamma e/Bb\alpha}$. This relation allows one to estimate γ as follows. In sample III, the distance of depinning $Y_{0,m} \approx \mathcal{L}$ has the same value as the period $p \approx 10^{-5}$ m (Table II), which yields $\gamma \approx \mathcal{L}^2 Bb\alpha/2e \approx 6\times10^{-12}$ N (with $B \approx 10^6$ N m^{-2}), a value similar to that found in mixtures of decyl-cyanobiphenyl/octyl-cyanobiphenyl (10CB/8CB) in Ref. [18] ($\gamma = 8\times10^{-12}$ N).

Coming now to the yield stress, we relate it to the pinning. An external stress σ acts on an edge dislocation through a PK force. Its value per unit length $F_{PK} = b\sigma$ is therefore counteracted by the pinning force due to the dots. One should then consider two different cases to estimate the magnitude of the pinning force. When $Y_{0,m} \ll N_s^{-1/2}$, that is, for a small density N_s of screw dislocations, we expect the

TABLE II. Characteristics of sample I and of the three samples represented in Fig. 8.

Sample	$e(\mu\text{m})$	α (rad)	$p(\mu\text{m})$	$\rho_m(\mu\text{m}^{-2})$	$\dot{\epsilon}_{jv}$ (s^{-1})	ν_{jv} (Hz) [a]	$\dot{\epsilon}_s(\text{s}^{-1})$	ν_s(Hz) [a]
I [b]	12	1.7×10^{-4}	22.5	3.7×10^{-3}				
II	10	1.6×10^{-4}	23.2	4.3×10^{-3}	5×10^{-4}	0.04	2×10^{-3}	0.15
III	8	2.9×10^{-4}	12.7	9.8×10^{-3}	2×10^{-4}	0.03	2×10^{-3}	0.30
IV	24	6.0×10^{-4}	6.7	6.2×10^{-3}	3×10^{-4}	0.05	6×10^{-4}	0.10

[a]The frequencies ν_i are related to the corresponding $\dot{\epsilon}_i$ in our experiments.
[b]The stationary regimes of plasticity were not reached because of the too high yield strain ε_0.

dislocation to be pinned on all dots closer than $\mathcal{L}\approx Y_{0,m}$ and the yield stress to be consequently of order

$$\sigma_0 \approx \mathcal{F} N_s \mathcal{L}/b. \tag{7}$$

However, when the typical distance between screw dislocations $N_s^{-1/2}$ becomes lower than $Y_{0,m}$, the number of pinning dots per unit length along the dislocation line scales as $N_s^{1/2}$ and the yield stress becomes

$$\sigma_0 \approx \mathcal{F} N_s^{1/2}/b. \tag{8}$$

Note finally that the measurements of yield strains in Table I provide a second way of estimating $\mathcal{F}$ through Eq. (7) and Eq. (8). We obtain in all cases $\mathcal{F}\approx10^{-11}$ N. This value is similar to the line tension of a dislocation pinned on a single point (see above). This result consolidates the hypothesis that the yield stress present in our experiments is entirely due to the pinning of edge dislocations.

B. Plastic regime

Beyond the yield strain ϵ_0, the sample exhibits a plastic regime: the edge dislocations move and reach a constant velocity v after a short transient regime (discussed below). This behavior is characteristic of the plasticity of crystals under stress and has been used to check the Orowan equation directly [21].

We observe two different regimes according to the value of $\dot{\epsilon}$. Below $\dot{\epsilon}_{jv}$ (see some values in Table II), the edge dislocations remain temporarily pinned, exhibiting a *jerky* motion during straining. The depinning distance $Y_{0,m}(\dot{\epsilon})$, however, decreases rapidly with increasing $\dot{\epsilon}$. Above $\dot{\epsilon}_{jv}$, the dislocations in the steady regime appear as parallel straight lines, the pinning dots are no longer observed, and the motion becomes *viscous*.

1. Orowan equation

For each sample, we have measured the stationary velocity acquired by the dislocations at different strain rate $\pm\dot{\epsilon}$ in both jerky and viscous regimes. We have therefore directly checked the Orowan equation (Fig. 8). In both regimes, the mean velocity follows the Orowan equation, and we find

$$\frac{\dot{\epsilon}}{\rho_m} = \delta v, \tag{9}$$

where δ=3.7 nm is close to the Burgers vector b measured at rest.

The Orowan equation is, however, not satisfied above the frequency ν_s (points A, B, and C in Fig. 8) where a transient regime becomes important and the distance covered by the dislocations during half a cycle decreases. In the limit of large frequencies (or strain rates), the dislocations are immobile, which corresponds to a pure elastic behavior.

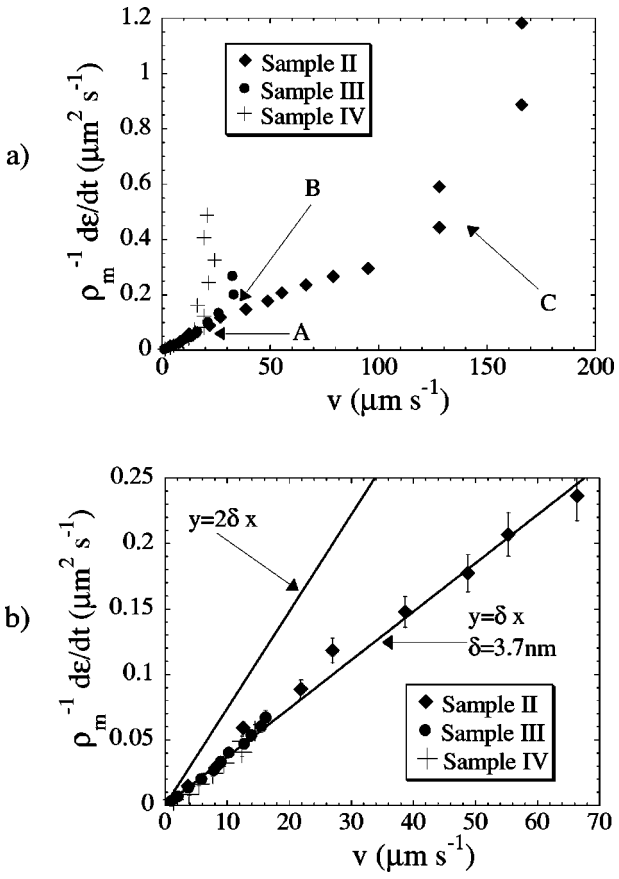

FIG. 8. (a) Evolution of $\dot{\epsilon}/\rho_m$ with the dislocation velocity v. Note that the Orowan relation [Eq. (2)] is well satisfied by a Burgers vector b=3.7 nm (close to the thickness of the smectic layers and to the static Burgers vector). Note also the departure from the Orowan relation at large velocities due to the existence of the relaxation time τ (see explanations in the text). The points A, B, and C denote the departure from the Orowan equation at large strain rate (frequencies greater than ν_s).

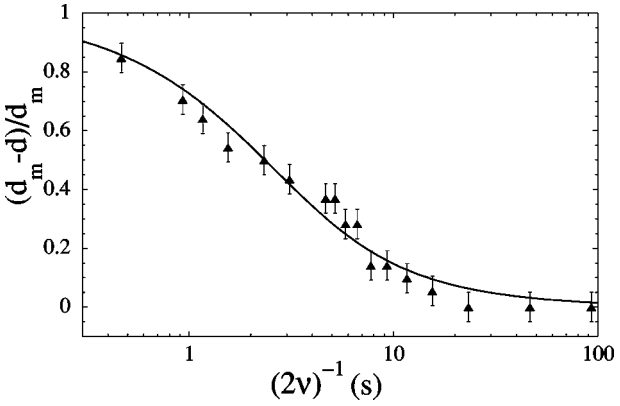

FIG. 9. Influence of the finite relaxation time τ upon the distance covered during half a cycle for sample III. The line is the best fit given by Eq. (13) with $\tau=1.47$ s.

2. Interpretation of the saturation regime

The saturation regime occurs when ν^{-1} is of the same order as the relaxation time τ necessary for a dislocation under constant strain rate to get a steady motion.

The equations of motion of the dislocations are given by [14]

$$v = M(\sigma - \sigma_0), \tag{10}$$

$$\sigma = B\epsilon_l = B\left(\dot{\epsilon}t - \frac{\int_0^t v\,dt\alpha}{e}\right), \tag{11}$$

where M is the mobility of an edge dislocation. We have added here a term σ_0 in the first equation to account for the observed pinning force. We assume that this force can be derived from the yield stress. The second equation gives the stress as a function of the local strain ϵ_l. Note that ϵ_l is different from the applied strain because the previous motion of edge dislocations has decreased the latter strain. Combining Eq. (10) and Eq. (11) yields a relaxation time τ:

$$\tau = \frac{e}{BM\alpha}. \tag{12}$$

The measurement of the instantaneous velocity was not accurate enough to measure τ. Let us then denote by d the distance covered by a dislocation during the duration $(2\nu)^{-1}$ of strain application. In the limit of a small pinning force σ_0 (which is the case for sample III), one gets

$$\frac{d_m - d}{d_m} = 2\tau\nu(1 - e^{-1/2\tau\nu}) \tag{13}$$

where d_m is the distance covered by the edge dislocations at low frequency (stationary regime). Using this equation, we found for sample III (see Fig. 9) $\tau=1.47$ s, of the order of $(2\nu_s)^{-1}=1.7$ s. The value of the mobility thus obtained, namely, $M\approx 1.9\times 10^{-8}$ m^2 s kg^{-1}, is in good agreement with recent measurements made in a free-standing Sm*A* film ($M\approx 4.4\times 10^{-8}$ m^2 s kg^{-1} for 8CB in Ref. [19]).

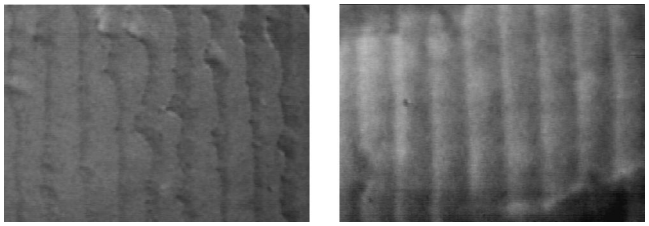

FIG. 10. Evolution of the morphology of the moving dislocation with the strain rate $\dot{\epsilon}$ for sample II. Left: For $\dot{\epsilon} < \dot{\epsilon}_{jv}$, a jerky motion due to the presence of pinning dots is observed. Right: For $\dot{\epsilon} > \dot{\epsilon}_j v$, a viscous motion is now observed and the pinning dots are no longer visible. Period of the array: 23.2 μm.

Note finally that the saturation regime, contrary to the pinning regime, is observed even at large strains. Because of the vicinity of the Sm*A*-Sm*C* transition, important deformations are made easier by the tilt of molecules visible through the formation of tilt domains.

C. The jerky-to-viscous transition

1. Observations

The morphology of the moving dislocation changes with the strain rate $\dot{\epsilon}$. Low values of the strain rate correspond to a jerky regime characterized by important variations with time of the edge dislocation velocity. Although the mean velocity follows Orowan's law, the instantaneous one varies strongly. When an edge dislocation meets a pinning dot, it suddenly stops. After its depinning, its velocity becomes much larger than the average and a straight line is rapidly reformed.

When the strain rate is increased above a value denoted $\dot{\epsilon}_{jv}$ in Table II, the pinning points are no longer observed, and the edge dislocation moves as a straight line (Fig. 10). We describe this regime as *viscous* in contrast with the *jerky* regime.

2. Interpretation of the transition

At first sight, our observations suggest that the pinning forces strongly decrease with increasing dislocation velocity, but a closer analysis shows that our observations remain compatible with a constant depinning force.

Let us consider a climbing dislocation crossing a dot during the stationary regime. Far from the pinning point, two forces act on the dislocation (see Fig. 11): a PK force $B\delta\epsilon_l\hat{\mathbf{y}}$ per unit length, where ϵ_l is the local strain at the position Y_0 and the opposing viscous force $-v\hat{\mathbf{y}}/M\mathbf{x}$, where M is the mobility of an edge dislocation in a sample without pinning points. In the vicinity of the pinning dot, the velocity drops rapidly to zero and the viscous force disappears. The profile of the dislocation is also due to the competition of the curvature force [see Eq. (5)] and the increased PK forces under stress. The shape is then given by

$$d\mathbf{F}_c + d\mathbf{F}_{PK} = \mathbf{0},$$

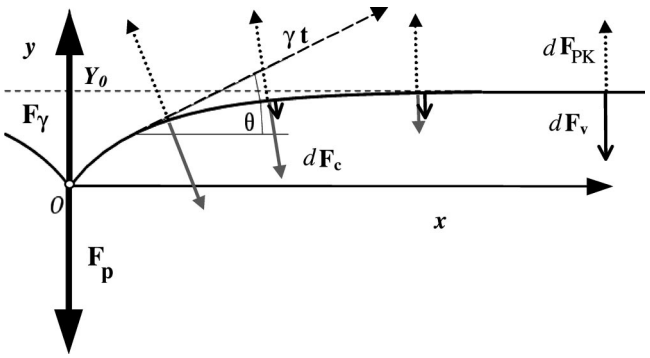

FIG. 11. Sketch of the forces acting on a climbing edge dislocation: PK force (dotted arrows), viscous force (plain black arrows), curvature force (plain gray arrows), and corresponding line tension (dashed arrows).

$$1-\cos\theta=\frac{(Y_0-y)^2}{\mathcal{L}^2}+K\epsilon_l\frac{Y_0-y}{\mathcal{L}}, \tag{14}$$

where $K=2e/\mathcal{L}\alpha$. The distance of depinning under stress $Y_{0,m}(\epsilon_l)$ is then related to the local strain ϵ_l by

$$Y_{0,m}^2=Y_{0,m}^2(\epsilon_l)+K\epsilon_l\mathcal{L}Y_{0,m}(\epsilon_l), \tag{15}$$

where $Y_{0,m}$ is the depinning distance at rest (≈ 10 μm). Therefore the length $Y_{0,m}(\epsilon_l)$ decreases rapidly with increasing ϵ_l. We have represented in Fig. 12 the evolution of the shape of two depinning dislocations [Eq. (14)] with ϵ_l for the typical values $\theta_0=\pi/4$, $K=10^4$ rad^{-1}, and a period p of 10 μm.

We arbitrarily define the jerky-viscous transition by the condition $Y_{0,m}(\epsilon_{l,jv})=Y_{0,m}/10$ (this corresponds to the optical resolution limit for the samples of Table II). The above static analysis gives the value of the local strain at the transition $\epsilon_{l,jv}\approx 10/K\approx 10^{-3}$. The more natural dynamical parameter $\dot{\epsilon}_{jv}=\rho_m bMB\epsilon_{l,jv}$ is then obtained through Eq. (9) and Eq. (10). Taking $\rho_m\approx 5\times 10^{-3}$ (data in Table II) we obtain $\dot{\epsilon}_{jv}\approx 3\times 10^{-4}$ s^{-1}, which is in good agreement with the data.

Note finally that this analysis shows that one should be careful about drawing conclusions about the interactions between screw and edge dislocations in motion from optical observations. Observations of straight edge dislocations moving in a smectic sample do not necessarily prove that the interaction is weak.

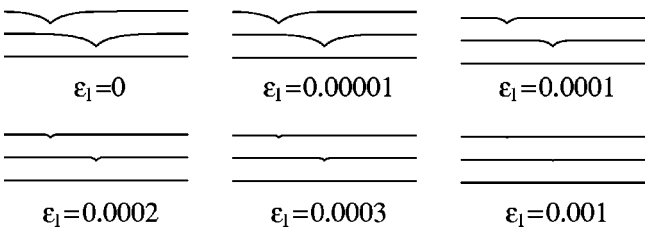

FIG. 12. Evolution of the shape of the depinning dislocations with the local strain ϵ_l.

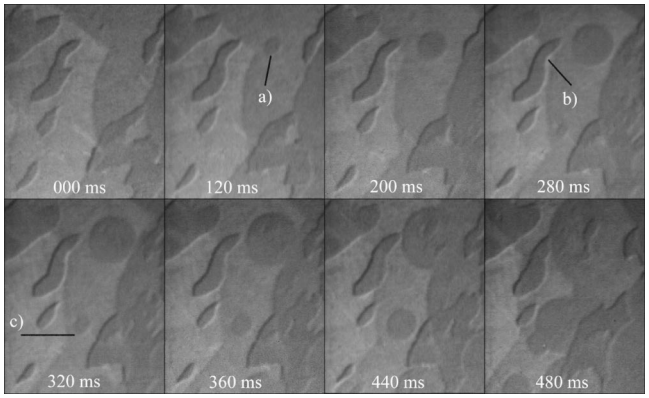

FIG. 13. Nucleation and growth of edge dislocation loops under compression (arrows *a* and *c*). Note that the other patterns (not necessarily circular) are domains of tilt which do not change with deformation.

D. Loop nucleation

An advantage of the setup we have used is the possibility of tuning ρ_m all over the sample. In the jerky and viscous regimes previously described, the liquid crystal contains enough mobile dislocations to relax the stress by their movement only. By decreasing the angle α, we can prevent this mechanism and favor the nucleation of edge dislocations.

1. Observations

We describe now a third regime in which the shape of edge dislocations greatly departs from straight lines. Figure 13 shows a series of pictures corresponding to a compression at a strain rate of 5×10^{-4} s^{-1} of a sample with a wedge angle $\alpha=2\times 10^{-5}$ rad. Due to the low density of edge dislocations, the stress is not rapidly relaxed, and the local strain becomes important, which is at the origin of two phenomena. First, tilt domains appear (due to the vicinity of the Sm*A*-Sm*C* transition) and become visible under crossed polarizers. They are usually noncircular (see point *b* in Fig. 13), which indicates that the corresponding line tension is rather low. Second, dislocation loops appear ahead of the edge dislocations and grow rapidly (points *a* and *c*). The loops disappear when they meet the next edge dislocation, with which they form a single line. Therefore, the main edge dislocations move forward indirectly through the nucleation of loops. The application of a periodical strain shows that the loops originate from fixed sources, apparently in the bisecting plane. Careful observations indicate, however, that no dust particles (of size at least larger than 1 μm) are present at the nucleation points.

This observation emphasizes the importance of dislocations with respect to the smectic flow. When the local angle between the plates is close to zero, no edge dislocations are present and the liquid crystal nucleates them in order to be able to flow.

2. Interpretation and discussion

We observed that the decrease of the angle α favors the nucleation of loops. In the limit $\alpha=0$ rad (perfectly parallel

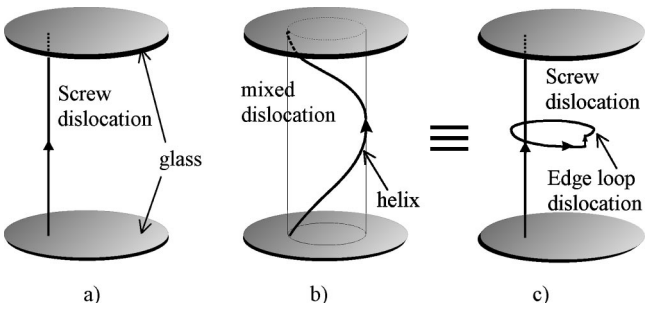

FIG. 14. Nucleation of a loop of edge dislocations from a screw dislocation, through a helical instability (see description in the text).

glasses), no other dislocations are indeed present and the nucleation of defects is unavoidable to remove one layer. This situation has been explored mainly in surface force experiments (see Refs. [9–12]) in which the separation of two parallel surfaces (plane and sphere or two cylinders) is slowly decreased. The resulting oscillatory plastic flow can be observed at macroscopic separations and is a consequence of the layered structure. References [9,10] discussed the mechanism responsible for the observed dynamics. Among several models, only the helical instability of screw dislocations was retained. Our observations strongly reinforce this model.

First, let us recall the proposed mechanism, which is described in detail in Refs. [13,14]. Figure 14 depicts the nucleation of a loop from a screw dislocation under a helical instability. Figure 14(a) represents a straight screw dislocation which joins the boundaries of an unstrained sample. Under compression, the screw dislocation is unstable and adopts a helical shape [Fig. 14(b)]. The origin of this instability comes from the fact that one layer has disappeared inside the cylinder formed by the helix, which therefore decreases the stress. The helical dislocation has acquired a mixed character (screw and edge) and can transform into a straight screw dislocation of the same Burgers vector plus a loop edge dislocation with a kink [Fig. 14(c)]. The loop then grows outward to relax the remaining stress.

The main characteristic of this model is that the edge loop should appear in the middle of the sample, around a screw dislocation, and should leave it unchanged, ready to nucleate another loop. Our observations are in complete agreement with these points and strengthen the validity of the helical instability model.

IV. DISCUSSION

Our results raise the problem of the microscopic origin of the pinning and how the dislocations intersect. We will now discuss this point further, which was already approached in Refs. [10,13,14] but is still unsolved. Note here that this discussion also concerns the bulk Sm*A* phase. To our knowledge, small Burgers vector edge dislocations in Sm*A* structures have not been observed at rest, but only indirectly in rapid motion because of the presence of tiny decorating focal conic domains (as reported in Ref. [13]). They were straight lines, but we have seen (Sec. III C 2) that pinning could nevertheless be present. References [9,10] clearly indicate that

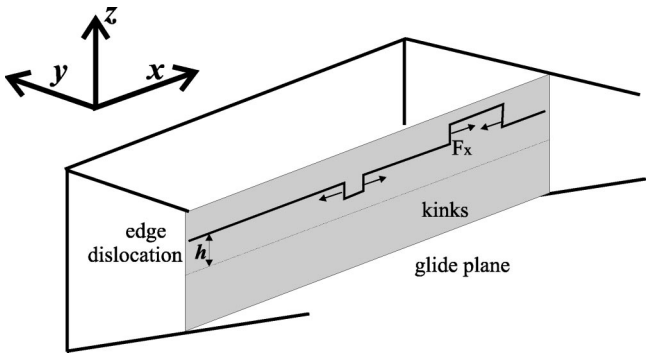

FIG. 15. Glide of an edge dislocation in the *x*-*z* plane through the motion of kinks.

the edge dislocations in a Sm*A* sample (8CB) are pinned. Therefore, we will consider defects in layered structures in a general way.

A. Influence of the wedge

First, we will discuss the influence of the wedge on the defects present in the bulk. Let us consider a dislocation shifted from the bisecting plane to a distance h. In a first approximation [27], the walls of the wedge act as two image dislocations located at the distance $e \pm 2h$ from the dislocation. The total interaction energy (per unit length and within the wedge) with the two image dislocations is [28]

$$E_I = \frac{1}{2}\frac{B\sqrt{\lambda}b^2}{4\sqrt{\pi}}\left(\frac{1}{\sqrt{e+2h}}+\frac{1}{\sqrt{e-2h}}\right)\approx\frac{B\sqrt{\lambda}b^2}{8\sqrt{\pi e}}\left(2+\frac{3h^2}{e^2}\right), \tag{16}$$

where λ is the smectic penetration length. The restoring force per unit length along $\hat{\mathbf{z}}$ is then

$$F_z = \frac{\partial E_I}{\partial h} = \frac{3B\sqrt{\lambda}b^2 h}{4\sqrt{\pi}e^{5/2}}. \tag{17}$$

This force is a PK force resulting from the stress generated by the image dislocations. It would yield a glide velocity along $\hat{\mathbf{z}}$:

$$v_g = \frac{M_g F_z}{b} = \frac{3M_g B\sqrt{\lambda}bh}{4\sqrt{\pi}e^{5/2}} \tag{18}$$

where M_g is the glide mobility. However, the dislocations are trapped in their Peierls-Nabarro valley, and an easy glide is possible only when $F_z > F_{PN}$, where the Peierls-Nabarro force F_{PN} is of order Bb per unit length. Here, a comparison with Eq. (17) shows that easy glide probably does not occur (note that this result has been shown directly for large-pitched cholesterics by fluorescence confocal polarizing microscopy [29]).

Another possible mechanism involves the nucleation and motion of kinks (see Fig. 15) as observed in cholesterics

[29]. The total force acting on a kink along $\hat{\mathbf{x}}$ and the corresponding velocity are (for a kink of elementary Burgers vector and height b)

$$F_x = \frac{\partial E_I}{\partial h} b = \frac{3B\sqrt{\lambda} b^3 h}{4\sqrt{\pi} e^{5/2}}, \tag{19}$$

$$v_k = \frac{M_k F_x}{b^2}, \tag{20}$$

where M_k is the kink mobility. This mechanism is certainly much more efficient in Sm*A* than in large-pitched cholesterics because of the very weak energy of such kinks (of order $Bb^3 \ll k_B T$ [30]), which can therefore appear spontaneously by thermal fluctuations. Let N_k be the number of pairs of kinks (two kinks of opposite signs) created along an edge dislocation per unit length and time. The net glide velocity resulting from the wedge is

$$v_g = \frac{3N_k MB\sqrt{\lambda} b^2 h}{4\sqrt{\pi} e^{5/2}}. \tag{21}$$

This efficient mechanism probably explains why the edge dislocations are always observed next to the bisecting plane in our experiments (the tilt boundary due to the edge is the lowest energy configuration).

B. Origin of the pinning force

Our observations have shown that the depinning force $\mathcal{F}$ is of the same order as the line tension γ of an edge dislocation: $\mathcal{F} = 2\gamma \sin\theta_{0,m}$ with $\theta_{0,m} \approx \pi/4$. In other words, the crossing is not easy (not thermally activated). This result is quite surprising because the crossing of a fixed screw dislocation of Burgers vector $\mathbf{b}_1$ by a moving perpendicular edge dislocation of Burgers vector $\mathbf{b}_2$ should give rise to a single kink on the edge dislocation of Burgers vector $\mathbf{b}_1$. The corresponding energy *far from the screw dislocation* is much lower than $k_B T$ and therefore the crossing is expected to be easy [31]. The complete problem of the interaction and the crossing between an edge and a screw dislocations seems, however, very complex to solve. We give below, as *simple illustrations*, two different effects which could intervene in this complex interaction.

1. Interaction between two rigid dislocations

In the linear approximation, there is no mean stress generated by a screw dislocation and thus no PK force acting on the edge dislocation. A similar problem concerning the interaction between two screw dislocations was discussed in Ref. [30] where the author shows that a long-range interaction arises from nonlinear terms. To have a glimpse of the nonlinear terms of the interaction between an edge and a screw dislocation, consider the strain $\epsilon_s \approx b_1^2/8\pi^2 r^2$ due to a single screw dislocation at a distance r from the core.

Applying the PK force formula to an edge dislocation located at the shortest distance R from the screw dislocation under normal stress $B\epsilon_s$, we get the net force

$$F_s = \frac{Bb_2 b_1^2}{8\pi R}. \tag{22}$$

Taking $B = 10^6$ N$\times$m^{-2} and $b_1 = b_2 = R = \delta$, we obtain $F_s \approx 10^{-12}$ N in the vicinity of the screw dislocation. This value shows that the elastic interaction could be sufficient to explain the pinning force that has been observed.

2. The role of the helical instability

Now reverse the above considerations, and consider the screw dislocation within the stress field generated by the edge dislocation. When the horizontal edge dislocation approaches the screw dislocation, this latter experiences a force in the vertical direction. As explained in Sec. III D, a screw dislocation might acquire some characteristics of an edge dislocation through the helical instability and form an edge dislocation loop.

The horizontal force per unit line between two elementary parallel edge dislocations is given by [28]

$$F = \pm \frac{B\delta^2}{8\pi} \frac{x_0}{z_0} \left(\frac{\pi}{\lambda z_0} \right)^{1/2} \exp\left(-\frac{x_0^2}{4\lambda z_0} \right), \tag{23}$$

where x_0 and z_0 are the horizontal and vertical displacements between the edge dislocations. During the localized interaction, we expect $x_0 \approx z_0 \approx \delta$ which yields for a loop of typical size δ, $F = B\delta^2$, which also has the right order of magnitude.

V. CONCLUSION

Direct observations under the microscope of the microscopic defects in a strained sample allowed us to confirm several hypotheses about the plasticity of smectics. Small deformations can be analyzed through the ''plasticity of solids'' approach. The intersections between screw and edge dislocation are not negligible and are at the origin of a small yield stress which depends strongly on the density of screw dislocations. Larger stresses are relaxed through the motion of edge dislocations in the bisecting plane of the wedge. Our experiment allowed us to check the Orowan equation directly and to determine the nature of its limits. The departure of the Orowan relation is mainly due to the finite mobility of the dislocations. When the stress is no longer relaxed by the preexisting defects, edge dislocation loops nucleate. Our observations strengthen the model of the helical instability of screw dislocations generating the loops.

The present experiment provides a unique tool for studying the local interactions between edge and screw dislocations during the compression of a lamellar material. From a macroscopic point of view, the plasticity of the sample results from the interaction between an array of elastic lines (the edge dislocations) and fixed obstacles (the anchored screw dislocations). Therefore, our system also seems very attractive for studying the physics of the depinning of an elastic line in a disordered landscape. For example, specific work could concern the phenomena related to the yield strain, such as avalanches (sudden depinning of several points) and other related phenomena.

ACKNOWLEDGMENTS

The authors would like to thank R. Ober of Collège de France for the small angle x-ray scattering measurement and M. Schaer (SFIT) for participating in surface characterization. We also acknowledge the financial support of Fonds National de la Recherche Scientifique (Switzerland). Finally, we would like to thank Professor F. R. N. Nabarro for useful comments on the presentation.

[1] E. Orowan, Proc. Phys. Soc. London **52**, 8 (1940).
[2] K. Sumino and K.I. Kojima, Cryst. Lattice Defects **2**, 159 (1971).
[3] M.J. Whelan, P.B. Hirsch, R.W. Horne, and W. Bollmann, Proc. R. Soc. London, Ser. A **240**, 524 (1957).
[4] D. Caillard and J.L. Martin, *Thermally Activated Mechanisms in Crystal Plasticity* (Elsevier, Amsterdam, 2003).
[5] P.-G. de Gennes and J. Prost, *The Physics of Liquid Crystals* (Clarendon Press, Oxford, 1993).
[6] M. Kleman and O.D. Lavrentovich, *Soft Matter Physics: An Introduction* (Springer-Verlag, New York, 2003).
[7] M. Kleman, Rep. Prog. Phys. **52**, 555 (1989).
[8] P. Oswald, Thèse d'état, University Paris–Sud, Orsay, France, 1985.
[9] R.A. Herke, N.A. Clark, and M.A. Handschy, Science **267**, 651 (1995).
[10] R.A. Herke, N.A. Clark, and M.A. Handschy, Phys. Rev. E **56**, 3028 (1997).
[11] R.G. Horn, J.N. Israechvili, and E. Perez, J. Phys. (France) **42**, 39 (1981).
[12] P. Richetti, P. Kekicheff, J.L. Parker, and B.W. Ninham, Nature (London) **346**, 252 (1990).
[13] L. Bourdon, M. Kleman, L. Lejcek, and D. Taupin, J. Phys. (France) **42**, 261 (1981).
[14] P. Oswald and M. Kleman, J. Phys. (France) Lett. **45**, L319 (1984); P. Oswald, Ph.D. thesis, University Paris-Sud, Orsay, France, 1985.
[15] F. Nallet and J. Prost, Europhys. Lett. **4**, 307 (1987).
[16] C. Quilliet, P. Fabre, and M. Veyssié, J. Phys. II **3**, 1371 (1993).
[17] R.B. Meyer, B. Stebler, and S.T. Lagerwall, Phys. Rev. Lett. **41**, 1393 (1978).
[18] The kinetics of loop dislocations has been recently studied during layer thinning in overheated smectic-*A* films. See J.C. Géminard, R. Holyst, and P. Oswald, Phys. Rev. Lett. **78**, 1924 (1997); S. Pankratz, P.M. Johnson, A. Paulson, and C.C. Huang, Phys. Rev. E **61**, 6689 (2000).
[19] F. Picano, R. Holyst, and P. Oswald, Phys. Rev. E **62**, 3747 (2000).
[20] I. Lelidis, M. Kleman, and J.L. Martin, Mol. Cryst. Liq. Cryst. Sci. Technol., Sect. A **330**, 457 (1999).
[21] I. Lelidis, M. Kleman, and J.L. Martin, Mol. Cryst. Liq. Cryst. Sci. Technol., Sect. A **351**, 187 (2000).
[22] Preliminary work mentioned in Refs. [20,21] used a silane treatment of the glass plates [F.J. Kahn, Appl. Phys. Lett. **22**, 386 (1973)]. This method seems to yield a higher density of screw dislocations in the sample.
[23] R. Bartolino and G. Durand, Phys. Rev. Lett. **39**, 1346 (1977).
[24] In order to detect all the pinning dots present in the sample, we proceed as follows. The sample is deformed at very small strain rate (frequency of order 10^{-3}–10^{-2} Hz) in the jerky regime (see Sec. III C 1). The slow motion of the edge dislocations crossing the pinning dots is recorded and all the pinning dots detected from the video recording. To improve the statistics, we observe several areas.
[25] I. Lelidis, C. Oedman, M. Kleman, and J.L. Martin (unpublished).
[26] M. Peach and J.S. Koehler, Phys. Rev. **80**, 436 (1950).
[27] Rigorously, the boundary conditions due to the wedge are not satisfied by two image dislocations but by an infinite set of dislocations located at $z=-me+(-1)^m h$ and $z=me+(-1)^m h$ (see Ref. [29]).
[28] M. Kleman and C. Williams, J. Phys. (France) Lett. **35**, L49 (1974).
[29] I.I. Smalyukh and O.D. Lavrentovich, Phys. Rev. E **66**, 051703 (2002).
[30] H. Pleiner, Liq. Cryst. **3**, 249 (1988).
[31] P. Oswald and P. Pieranski, *Les Cristaux Liquides* (Gordon and Breach Science Publishers, Paris, 2002), Vol. 2, p. 141.